JOURNAL OF SOLID STATE CHEMISTRY 23, 115–129 (1978)

$FeBO_3$ Solid Solutions: Synthesis, Crystal Chemistry, and Magnetic Properties*

OLAF MULLER, MICHAEL P. O'HORO, AND JAMES F. O'NEILL

Xerox Corporation, Webster Research Center, Webster, New York 14580

Received May 14, 1977; in revised form June 14, 1977

Solid solutions of the type $Fe_{1-x}M_xBO_3$ have been prepared where M = Mn, Cr, Al, Ga, or In. For M = In, Ga, or Cr, x can vary from 0 to 1.0, but the solid solution range is more restricted for M = Al ($0 \leq x \leq 0.32$) and Mn ($0 \leq x \leq 0.10$). The present investigation of these materials includes their crystal chemistry, thermal stability, and magnetic properties. The calcite-type unit-cell parameters follow closely Vegard's Law. DTA results indicate that the thermal stability increases with increasing M content for M = Cr, Al, or In. Room-temperature magnetic measurements show that the $Fe_{1-x}M_xBO_3$ phases remain canted antiferromagnets up to the 20 to 30% substitution level, with monotonic decrease in the magnetization and Curie temperature as a function of the concentration of M (dilution effect). Low-temperature magnetic studies of the systems $Fe_{1-x}Cr_xBO_3$ and $Fe_{1-x}In_xBO_3$ show anomalous magnetic behavior at the higher Cr and In concentrations.

Introduction

Green $FeBO_3$ has the calcite structure with trivalent iron in a slightly distorted octahedral environment. It is one of the very few room-temperature ferrimagnetic materials which is transparent well into the visible. Although the compound was first described by Bernal *et al.* in 1963 (*1*), it was not until 1968 that the magnetic properties were shown to be intrinsic to $FeBO_3$ (*2*), rather than arising from impurities, as had been previously suspected. More recent magneto-optic studies of flux-grown single $FeBO_3$ crystals (*3–5*) have shown that $FeBO_3$ has a magnetization $4\pi M$ of 115 G at room temperature, a Curie temperature of 348°K, and a prominent absorption window in the green (5250 Å) with $\alpha = 39\ cm^{-1}$. With a large Faraday rotation of 2300° per centimeter at 5250 Å, a number of potential magneto-optic applications have been suggested for $FeBO_3$ (*3–5*).

This combination of interesting properties has stimulated additional research on $FeBO_3$ on optical and magneto-optical properties (*6–16*), crystal growth and phase relations (*17–19*), crystal structure refinement (*20*), magnetic structure (*21*), NMR (*22–24*), and Mössbauer spectroscopy (*25*).

Although the literature on pure $FeBO_3$ is quite extensive, little is known about $FeBO_3$ solid solutions. Aside from a few solid solutions reported in the original work of Bernal *et al.* (*1*), only a small number of additional compositions have been synthesized and studied:

(a) $Fe_{0.98}Al_{0.02}BO_3$ plus impure samples possibly in the range $Fe_{0.3}Al_{0.7}BO_3$–$Fe_{0.6}Al_{0.4}BO_3$, all prepared at high pressures (*26*).

(b) A 1.5 atom% In-substituted $FeBO_3$ phase for which Raman spectra have been collected (*10*).

(c) $Fe_{0.9}Ga_{0.1}BO_3$ crystals for which again Raman data are available (*13*).

(d) $Fe_{1-x}Ga_xBO_3$ with $x = 0.18$, 0.3, and 0.4 for which NMR studies have been carried out (*22, 24*).

* A preliminary account of this work was given at the 78th Annual Meeting of the American Ceramic Society, May 5, 1976. Abstract 95-B76, *Amer. Ceram. Soc. Bull.* 55, 402 (1976).

0022-4596/78/2312-0115$02.00/0

TABLE I

FINAL HEAT TREATMENT, DECOMPOSITION TEMPERATURES, AND UNIT-CELL PARAMETERS FOR $Fe_{1-x}M_xBO_3$ SOLID SOLUTIONS

Composition[a]	Final heat treatment		T (decomp)[b] (°C)	Cell parameters[c]	
	Length	T (°C)		a_0 (Å)	c_0 (Å)
$FeBO_3$	4 weeks	810	916	4.626(2)	14.480(4)
$Fe_{0.978}Al_{0.022}BO_3$	18 days	810	938	4.621 (2)	14.468(3)
$Fe_{0.95}Al_{0.05}BO_3$	26 days	810	960	4.619(1)	14.454(4)
$Fe_{0.90}Al_{0.10}BO_3$	16 days	805	966	4.612(2)	14.427(4)
$Fe_{0.79}Al_{0.21}BO_3$	24 days	795	981	4.596(2)	14.358(4)
$Fe_{0.73}Al_{0.27}BO_3$	26 days	810	987	4.589(1)	14.319(2)
$Fe_{0.97}Ga_{0.03}BO_3$	24 days	810	926	*d*	*d*
$Fe_{0.95}Ga_{0.05}BO_3$	15 days	810	940	4.623(2)	14.468(3)
$Fe_{0.91}Ga_{0.09}BO_3$	5 days	805	956	4.621(2)	14.455(4)
$Fe_{0.80}Ga_{0.20}BO_3$	5 days	805	990	4.617(1)	14.439(3)
$Fe_{0.69}Ga_{0.31}BO_3$	15 days	810	1013	4.609(1)	14.399(1)
$Fe_{0.60}Ga_{0.40}BO_3$	15 days	810	1019	4.605(1)	14.374(2)
$Fe_{0.51}Ga_{0.49}BO_3$	5 days	805	1018	4.599(1)	14.347(2)
$Fe_{0.41}Ga_{0.59}BO_3$	15 days	810	1005	4.594(1)	14.319(3)
$Fe_{0.21}Ga_{0.79}BO_3$	15 days	810	989	4.582(1)	14.252(2)
$Fe_{0.993}In_{0.007}BO_3$	9 days	810	955	4.628(1)	14.483(3)
$Fe_{0.978}In_{0.022}BO_3$	13 days	805	966	4.631(1)	14.511(2)
$Fe_{0.92}In_{0.08}BO_3$	9 days	810	961	4.641(1)	14.559(3)
$Fe_{0.87}In_{0.13}BO_3$	5 days	805	963	4.652(2)	14.632(2)
$Fe_{0.74}In_{0.26}BO_3$	5 days	805	998	4.677(2)	14.767(10)
$Fe_{0.62}In_{0.38}BO_3$	1 hour	920	1050	4.702(2)	14.864(12)
$Fe_{0.51}In_{0.49}BO_3$	20 days	855	—	4.724(1)	14.979(10)
$Fe_{0.43}In_{0.57}BO_3$	16 days	805	—	4.741(2)	15.085(10)
$Fe_{0.42}In_{0.58}BO_3$	6 days	930	—	4.743(1)	15.065(8)
$Fe_{0.35}In_{0.65}BO_3$	20 days	855	—	4.760(1)	15.154(3)
$Fe_{0.15}In_{0.85}BO_3$	24 days	795	—	4.793(1)	15.311(1)
$Fe_{0.042}In_{0.958}BO_3$	20 days	855	—	4.816(2)	15.415(3)
$Fe_{0.98}Cr_{0.02}BO_3$	24 days	810	922	*d*	*d*
$Fe_{0.95}Cr_{0.05}BO_3$	26 days	810	947	4.624(1)	14.468(5)
$Fe_{0.89}Cr_{0.11}BO_3$	24 days	795	970	4.620(2)	14.454(3)
$Fe_{0.80}Cr_{0.20}BO_3$	24 days	795	1023	4.616(1)	14.440(2)
$Fe_{0.70}Cr_{0.30}BO_3$	9 days	810	1055	4.612(2)	14.419(3)
$Fe_{0.60}Cr_{0.40}BO_3$	6 days	930	1087	4.608(2)	14.392(2)
$Fe_{0.50}Cr_{0.50}BO_3$	24 days	795	1123	4.603(1)	14.378(5)
$Fe_{0.50}Cr_{0.50}BO_3$	6 days	930	—	4.602(1)	14.369(2)
$Fe_{0.40}Cr_{0.60}BO_3$	6 days	930	1153	4.597(1)	14.345(3)
$Fe_{0.19}Cr_{0.81}BO_3$	9 days	810	1208	4.589(2)	14.300(2)
$Fe_{0.05}Cr_{0.95}BO_3$	6 days	930	1264	4.580(2)	14.263(3)
$Fe_{0.995}Mn_{0.005}BO_3$	24 days	810	—	*d*	*d*
$Fe_{0.989}Mn_{0.011}BO_3$	24 days	810	—	*d*	*d*
$Fe_{0.979}Mn_{0.021}BO_3$	5 days	805	—	*d*	*d*
$Fe_{0.95}Mn_{0.05}BO_3$	24 days	810	—	*d*	*d*
$Fe_{0.92}Mn_{0.08}BO_3$	5 days	805	—	4.626(3)	14.479(4)

In view of the paucity of information involving solid solutions, we felt that a systematic study should be made of several $Fe_{1-x}M_xBO_3$ systems in which the magnetic properties (magnetization, Curie temperature, etc.), and cell parameters can be correlated with composition. By studying such property/composition relationships, one can hope to gain a better understanding of these interesting materials.

In this paper we present a comprehensive study of $Fe_{1-x}M_xBO_3$ solid solutions where M = Mn, Cr, Al, Ga, and In.

Synthesis

Our first objective was to find an easy way of preparing green polycrystalline $FeBO_3$ powders. It is known that flux-grown $FeBO_3$ crystals can be either green (transparent) or more opaque brown (*3, 5, 24*). $FeBO_3$ powders prepared by sintering Fe_2O_3 and H_3BO_3 according to the method of Joubert *et al.* (*2*) were described as yellow brown. Our attempts to make $FeBO_3$ powders according to Joubert's method (*2*) always resulted in brown $FeBO_3$ powders contaminated with small but detectable quantities of α-Fe_2O_3.

After several trials, a method was found which was generally suitable not only for making green $FeBO_3$, but also for preparing solid solutions of the type $Fe_{1-x}M_xBO_3$ where M = Mn, Cr, Al, Ga, and In. The appropriate hydrated metal nitrates are dissolved with a 400% excess H_3BO_3 in hot deionized water. The solutions are then slowly evaporated to dryness over a hot plate with occasional stirring. When the resulting crust is dry, the material is ground, powdered, and mixed thoroughly under acetone to achieve greater homogeneity. Upon drying, homogeneous brown amorphous powders are obtained which serve as precursors to the final $Fe_{1-x}M_xBO_3$ products. These powders are loaded into platinum crucibles, and heated slowly from 200 to 500°C and maintained at 500°C for about 12 hr. Finally the products are fired in air at higher temperatures and for more prolonged time spans, typically 3 weeks at 810°C. After air quenching, the $Fe_{1-x}M_xBO_3$ samples are freed from the excess B_2O_3 by repeatedly washing with water.

The precise duration and temperature of the final heat treatment is not critical, but for compositions close to $FeBO_3$ the firing should take place for about 3 weeks at 810°C. If such a heat treatment is interrupted after only 1 or 2 days, significant amounts of Fe_3BO_6 impurities are present, as seen from their characteristic X-ray pattern (*27*) and the brown discoloration of the product. Apparently the reaction takes place in two stages. First the amorphous iron oxide reacts with B_2O_3 to form Fe_3BO_6 within about 10 min. Subsequently the brown Fe_3BO_6 reacts much more slowly with additional B_2O_3 to form green $FeBO_3$. Such a reaction sequence has recently been described by Jach (*28*) and was confirmed in this study with a few trial experiments where the precursor iron borate powders were heated for varying lengths of time at 800°C and also at higher and lower temperatures. At temperatures significantly below 800°C, conversion to $FeBO_3$ is even slower whereas temperatures much higher than 810°C cause $FeBO_3$ to decompose. (See the proposed phase diagrams for the system Fe_2O_3–B_2O_3 (*2, 18*).)

With increasing M content, $Fe_{1-x}M_xBO_3$ solid solutions become thermally more stable.

---

[a] The compositions listed here are based on chemical analyses.

[b] The decomposition temperatures given here are based on DTA runs using a heating rate of 2°C per minute.

[c] Given here are the hexagonal cell parameters of the rhombohedral calcite-type solid solutions. Parentheses are used to indicate the estimated uncertainty in the last decimal place(s).

[d] These phases have cell constants very close to those of pure $FeBO_3$; however, no slow scan X-ray patterns were taken for these compounds.

Therefore higher reaction temperatures and shorter time spans can be used. In Table I we list the actual heat treatment applied to the various $Fe_{1-x}M_xBO_3$ samples used in the present study. All such samples were single-phase $Fe_{1-x}M_xBO_3$ powders with the calcite structure and with no impurities detectable by X-ray diffraction.

It has been our experience that heating the $Fe_{1-x}M_xBO_3$ precursor mixes (where $x = 0$ or very small) at 810°C for only a few days will result in the formation of calcite type $Fe_{1-x}M_xBO_3$ as the primary phase but with detectable amounts of Fe_3BO_6 also present. To eliminate these impurities may require a continuation of the heat treatment for 2 or 3 weeks longer.

We have found a way to shorten the reaction time by the simple expedient of adding some $LiNO_3$ or $NaNO_3$ to the aqueous solution of iron nitrate and boric acid. Even the addition of 1 mole of $LiNO_3$ or $NaNO_3$ for every 50 moles of $Fe(NO_3)_3 \cdot 9H_2O$ allows one to prepare pure $FeBO_3$ with a heat treatment of only 2 days at 810°C[1]. The alkali metal ions serve to lower the viscosity of the B_2O_3 flux and thereby increase the reaction rate. The alkali metal ions do not enter into the calcite-type $FeBO_3$ structure, but stay in the excess B_2O_3 flux. The products obtained by this method are indistinguishable in appearance, X-ray pattern and magnetic properties from the products obtained without the use of alkali. No Li^+ or Na^+ could be detected in these $FeBO_3$ powders by flame photometry. Typical analaysis result: 48.82 wt% Fe, below 0.0001 wt% Li. Calculated for $FeBO_3$: 48.71 wt% Fe.

Solid Solution Range

In Fig. 1 we illustrate the extent of the $Fe_{1-x}M_xBO_3$ solid solution range where M = Mn, Al, Cr, Ga, and In. Also given are the colors of the polycrystalline samples.

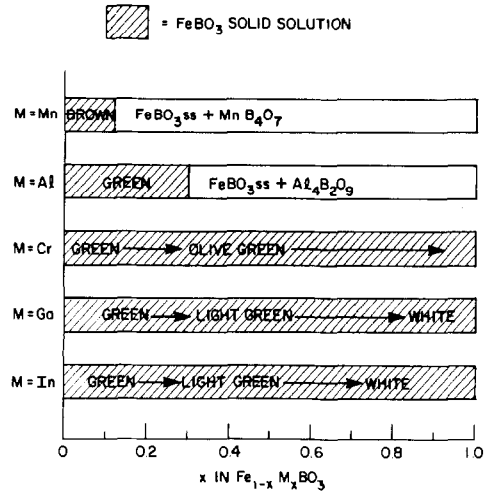

FIG. 1. Solid solution range of $Fe_{1-x}M_xBO_3$.

In the $Fe_{1-x}Mn_xBO_3$ system, we were able to obtain pure calcite-type phases only up to $x = 0.08$, and we estimate that the calcite structure is not stable much beyond the $Fe_{0.90}Mn_{0.10}BO_3$ composition. With further increase in the Mn-content, a second phase was detected in the X-ray pattern which has been identified as paramagnetic MnB_4O_7 (*29*). The very limited amount of solid solution can be attributed to the low stability of Mn^{3+} in these borate systems at 800°C, and to the fact that Mn^{3+} shows Jahn–Teller distortions with a preference for a strongly distorted octahedral site, whereas in the calcite structure of $FeBO_3$, Fe^{3+} has a nearly perfect octahedral environment (*20*). The Mn-substituted iron borates are less transparent than the other compositions listed in Table I. While $Fe_{0.995}Mn_{0.005}BO_3$ is still dark olive green, all other Mn-substituted phases listed in Table I are brown.

In the $Fe_{1-x}Al_xBO_3$ system, pure calcite-type phases could be obtained up to $x = 0.27$. Beyond that composition, traces of $Al_4B_2O_9$ (*30*) were detected in the X-ray pattern and under the microscope. From a knowledge of the unit-cell parameters of the $Fe_{1-x}Al_xBO_3$ phase ($a_0 = 4.578$ Å, $c_0 = 14.283$ Å) which is in equilibrium with $Al_4B_2O_9$ at 800°C we

[1] Even in this case, traces of very fine Fe_3BO_6 may persist (brown streaks). However, on washing, the very fine brown Fe_3BO_6 can be suspended in the water and decanted with the water, whereas the much coarser green platy $FeBO_3$ settles quickly to the bottom of the beaker. With a few such washings, $FeBO_3$ can be obtained free from any detectable trace of Fe_3BO_6.

estimate the maximum Al content at $x = 0.32$. The restricted solid solution range of $AlBO_3$ in $FeBO_3$ is not surprising in view of the fact that the calcite-type $AlBO_3$ end member can be prepared only at high pressures (*26*, *31*) due to the small size of the Al^{3+} ion. It is interesting to note that Bither and Young (*26*) were apparently unable to prepare (at high pressures) $Fe_{1-x}Al_xBO_3$ solid solutions between $x = 0.03$ and $x = 0.32$. They further describe impure, dark-colored calcite-type samples possibly in the range $Fe_{0.3}Al_{0.7}BO_3$ to $Fe_{0.6}Al_{0.4}BO_3$. Judging from their dark appearance, these products probably are partly reduced. All of our samples from $FeBO_3$ to $Fe_{0.68}Al_{0.32}BO_3$ are green to light green, and one would expect that further Al-substitution would yield sample colors with even lighter shades of green.

There is apparently complete solid solution in the systems $Fe_{1-x}Cr_xBO_3$, $Fe_{1-x}Ga_xBO_3$, and $Fe_{1-x}In_xBO_3$ where x can vary from 0 to 1.0, as seen from Table I and Fig. 1. This is not unexpected in view of the existence of calcite-type $CrBO_3$ (*32*, *33*), $GaBO_3$ (*26*, *31*), and $InBO_3$ (*34*). The $Fe_{1-x}Cr_xBO_3$ samples were all green to olive green throughout the composition range. The $Fe_{1-x}Ga_xBO_3$ and $Fe_{1-x}In_xBO_3$ phases are green near the $FeBO_3$ composition, changing toward lighter shades of green as more In and Ga are added until the samples grade into white as the $GaBO_3$ and $InBO_3$ compositions are approached. For example, while $Fe_{0.35}In_{0.65}BO_3$ is still very light green, $Fe_{0.15}In_{0.85}BO_3$ is best described as white with a barely perceptible green tinge. The composition $Fe_{0.042}In_{0.958}BO_3$ is pure white.

Analysis Results

A metal ion analysis for Fe and M in $Fe_{1-x}M_xBO_3$ was performed for all compositions listed in Table I, and the formulas in that table are based on these analysis results. The samples were dissolved in $K_2S_2O_7$ flux and the analyses were performed by several different techniques, including atomic absorption, differential pulse polarography, and wet chemical methods. We felt that such an analysis was essential because of the uncertainty regarding the extact stoichiometry of the hygroscopic hydrated metal nitrate starting materials. Furthermore, one of the metal ions might be more soluble in the excess borate flux than the other component. Only in the case of the $Fe_{1-x}In_xBO_3$ solid solutions did we find significant discrepancies between those formulas based on the analyses and those corresponding to the weight of the metal nitrate starting components. For most samples, the calculated recovery ranged between 99 and 101% based on the assumption of the formula $Fe_{1-x}M_xBO_3$. No analyses were performed for boron and oxygen.

Thermal Decomposition

DTA data were taken on a DuPont 990 Thermal Analyzer for most of our samples. Our objective was to monitor the decomposition temperatures of the various $Fe_{1-x}M_xBO_3$ solid solutions. A heating rate of 2°C per minute was used and a clear exothermic peak was obtained. The decomposition temperature was determined by the usual extrapolated onset method. The results are shown in Table I and are plotted in Fig. 2. For the $Fe_{1-x}In_xBO_3$ solid solutions beyond $x = 0.38$ the DTA signal became too weak to be detected; hence no decomposition temperatures are listed for such phases in Table I.

It is apparent that the phases become thermally more stable as Fe^{3+} is replaced by Cr^{3+}, Ga^{3+}, Al^{3+}, or In^{3+}. The decomposition temperatures increase with increasing content of M except for the $Fe_{1-x}Ga_xBO_3$ system where a broad maximum is reached around $x = 0.40$. This is in agreement with the higher temperatures used in the synthesis of pure $CrBO_3$ (*32*) and $InBO_3$ (*34*) and the lower temperatures at which pure $GaBO_3$ is prepared (*26*).

The anomalously high decomposition temperatures for $Fe_{0.993}In_{0.007}BO_3$ and $Fe_{0.978}In_{0.022}BO_3$ are unexpected and can

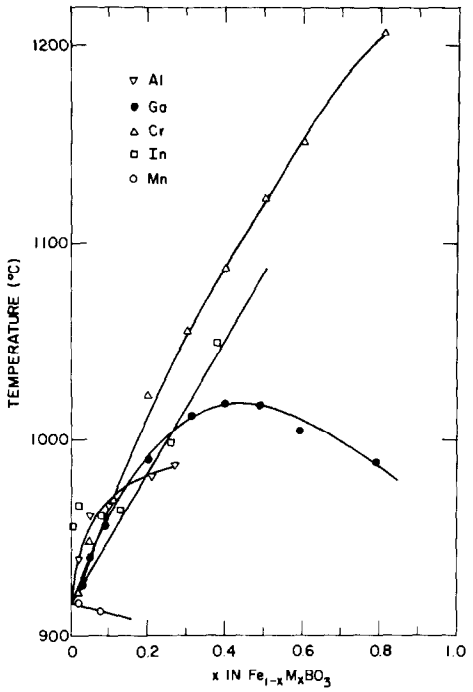

FIG. 2. Decomposition temperatures of various $Fe_{1-x}M_xBO_3$ solid solutions.

perhaps be partly explained on the basis of crystal size. These two compositions are more coarsely crystallized, whereas the other In-substituted phases are more finely divided and therefore decompose at comparatively low temperatures.

The decomposition temperatures listed in Table I and Fig. 2 are, of course, not true equilibrium decomposition temperatures which may actually be lower by 50 to 100°C than the values listed in Table I. Nevertheless these data are useful guides in selecting potential sintering temperatures for the preparation of solid solutions of any given composition.

Attempts were made to find the true equilibrium decomposition temperatures for $FeBO_3$ and a few substituted solid solutions. This proved to be difficult due to the very slow rates at which equilibrium can be reached.

When the precursor $FeBO_3$ powder is heated for 16 days at 860°C only Fe_3BO_6 and B_2O_3 are obtained. However when well-crystallized green $FeBO_3$ is subjected to the same heat treatment, the crystals turn partly brown, but the calcite structure and cell dimensions of $FeBO_3$ are retained with only a trace of Fe_3BO_6 detectable in the X-ray pattern. Under these conditions the decomposition of green $FeBO_3$ (to Fe_3BO_6 and B_2O_3) may proceed very slowly over a brown (non-stoichiometric?) $FeBO_3$ intermediate. After green $FeBO_3$ has been heated for 1 day at 880°C, the decomposition to Fe_3BO_6 and B_2O_3 is virtually complete; however, even this temperature is well below the 916°C derived by DTA and 910°C given by Zvereva *et al.* (*19*). Similar results have been obtained for some other $Fe_{1-x}M_xBO_3$ compositions.

It is apparent that excess B_2O_3 helps to prevent $Fe_{1-x}M_xBO_3$ phases from decomposing. In several cases we have observed that when precursor powders or $Fe_{1-x}M_xBO_3$ samples mixed with excess B_2O_3 are heated near the decomposition temperature in a closed environment, no discoloration or decomposition takes place. However, when the corresponding $Fe_{1-x}M_xBO_3$ samples alone are heat treated under the same conditions in an open platinum dish or foil, the samples tend to discolor and partially decompose due to a loss of the volatile B_2O_3. In view of these observations it is recommended that a large excess of B_2O_3 be present when $Fe_{1-x}M_xBO_3$ samples are prepared.

X-Ray Diffraction Study

All samples were routinely X-rayed to insure that no impurities were present. A Siemens diffractometer was used with Cu$K\alpha$ radiation. Sample smears were mounted on glass slides. Preferred orientation was commonly observed with the hexagonal (00*l*) reflections abnormally intense due to the platy habit found for most samples. For most samples in Table I, internally standardized slow-scan X-ray patterns were taken and seven to ten peaks were used to derive the hexagonal a_0 and c_0 parameters for these rhombohedral phases. These values are listed in Table I and are also plotted as a function of composition in Figs. 3 and 4. As can be seen,

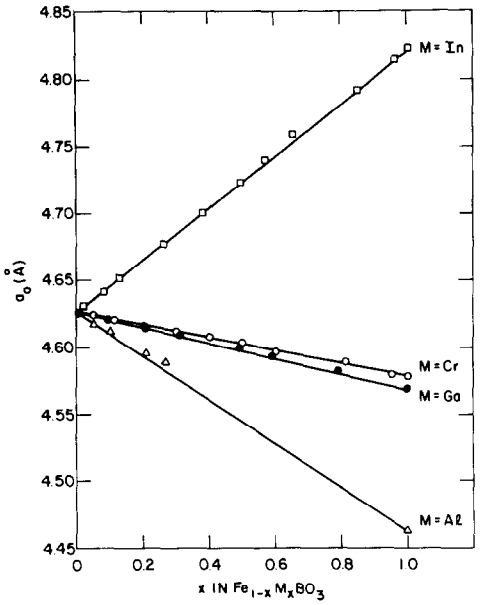

FIG. 3. Hexagonal a_0 parameter as a funciton of x in $Fe_{1-x}M_xBO_3$.

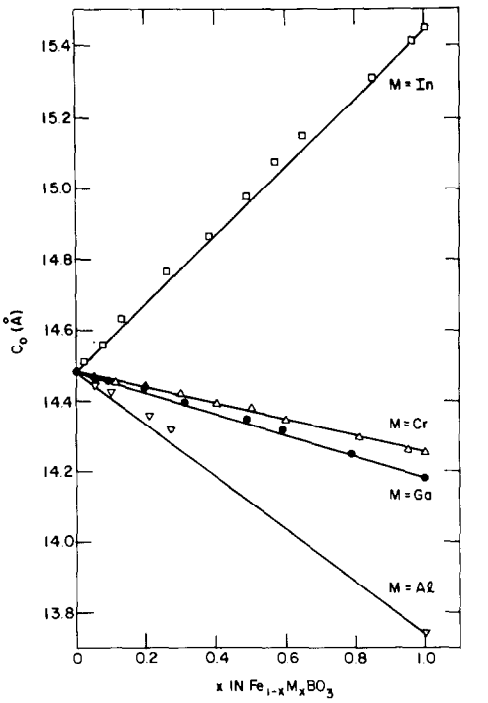

FIG. 4. Hexagonal c_0 parameter as a function of x in $Fe_{1-x}M_xBO_3$.

the plots are nearly linear, in close agreement with Vegard's law, although in the case of $Fe_{1-x}In_xBO_3$ and $Fe_{1-x}Al_xBO_3$ small deviations do occur from such an ideal linear relationship. The end-member compounds $InBO_3$, $GaBO_3$, $CrBO_3$, and $AlBO_3$ were not prepared in this study; their cell constants plotted in Figs. 3 and 4 were taken from the literature (*26*, *32*, *34*).

The cell parameters given for $Fe_{0.9}Ga_{0.1}BO_3$ by Bernal *et al.* (*1*) are not in good agreement with our parameters for a similar composition, but appear to correspond to a higher Ga content. Bernal *et al.* (*1*) further state that all of the different compositions prepared by them have the same cell constants as $Fe_{0.9}Ga_{0.1}BO_3$. This is in sharp disagreement with our own findings. Our cell constants for $FeBO_3$ are in good agreement with the values reported in the literature (*2*, *19*, *20*).

The cell parameters for all $Fe_{1-x}M_xBO_3$ solid solutions are in excellent accord with the known ionic radii (*35*). The observation that $Fe_{0.92}Mn_{0.08}BO_3$ has the same cell parameters as pure $FeBO_3$ can be attributed to the fact that Mn^{3+} and Fe^{3+} have equal ionic radii (*35*).

Magnetic Measurements

$FeBO_3$ is a canted antiferromagnetic material in which the Fe^{3+} spins are canted slightly from collinear antiparallel alignment, the spins being strictly oriented within the hexagonal (001) planes or rhombohedral (111) planes, as required by symmetry arguments (*5*, *21*). The canting results in a small net moment perpendicular to the threefold c-axis with a cant angle of 0.92° (*22*), giving rise to a net magnetization at room temperature of 115 G (2.15 emu/g). The hard axis [001] anisotropy field for $FeBO_3$ at room temperature is 63 000 Oe, whereas the in-plane (001) anisotropy field is below 1 Oe. The Curie temperature determined from single-crystal data is 348°K (*5*).

Canting on the Fe^{3+} sublattice is a consequence of the competition between the symmetric exchange coupling $J\bar{S}_1 \cdot \bar{S}_2$ which favors antiparallel spin alignment and weaker antisymmetric exchange couplings $\bar{D} \cdot (\bar{S}_1 \times \bar{S}_2)$ with a spin alignment perpendicular to the above (*36*). The cant angle γ is given by the

relation: $\tan 2\gamma = D/J$, and the magnetization by $M_s = 2M_0 \sin \gamma \approx M_0 D/J$ where M_0 is the sublattice magnetization. Decreasing J is seen to increase the cant angle and consequently the net moment. The value of D is related to the strength of the spin–orbit interaction.

Magnetization measurements of the $Fe_{1-x}M_xBO_3$ materials discussed in this paper were made with a vibrating sample magnetometer (Princeton Applied Research Inc.) from 4.2 to 600°K in fields up to 14 kOe. The magnetization results are accurate to within 2%. All of the samples measured were in the form of polycrystalline powders, mostly of a platelike habit. Powders made up predominantly of larger platelike crystallites (10–100 μm across) show preferential packing in the magnetometer sample holder, such that the (001) planes of the crystallites tend to be oriented parallel to the direction of the applied field. Samples containing smaller (below 5 μm) more compact crystallites approached a more random orientation in the sample holder.

Due to the large magnetic anisotropy of $FeBO_3$, the observed moment of a polycrystalline powder will be lower than the corresponding single-crystal value measured with the field perpendicular to the [001] axis. For randomly oriented $FeBO_3$ powders the relationship (5) is: $\sigma_p = (\pi/4)\sigma_s$. Our magnetization measurements on a number of polycrystalline $FeBO_3$ powders having a platy habit show a zero-field saturation moment which is 10 to 12% lower than the reported single-crystal value of 2.15 emu/g, in accordance with the high preferred orientation expected from powders with such a platy habit. All of the magnetization values reported in this paper represent measurements made on such powders and have not been corrected to single-crystal values.

In Figs. 5 and 6 we show the room-temperature magnetization as a function of applied field for $Fe_{1-x}In_xBO_3$ and $Fe_{1-x}Cr_xBO_3$, respectively. Similar curves were obtained for the $Fe_{1-x}Al_xBO_3$,

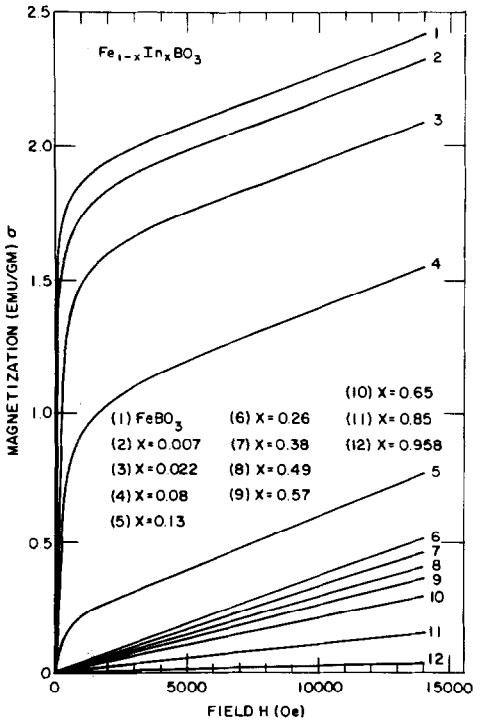

FIG. 5. Magnetization curves at room temperature of $Fe_{1-x}In_xBO_3$ solid solutions.

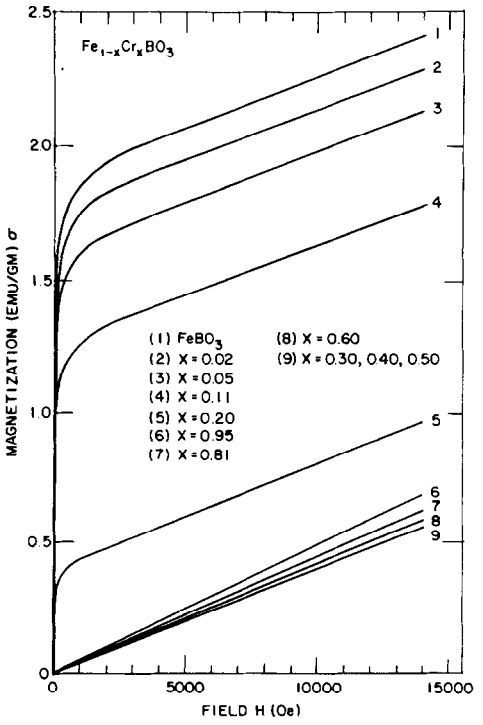

FIG. 6. Magnetization curves at room temperature of $Fe_{1-x}Cr_xBO_3$ solid solutions.

TABLE II
MAGNETIC DATA FOR $Fe_{1-x}M_xBO_3$ SOLID SOLUTIONS

Composition	Room temperature magnetization σ (emu/g) at 1000 Oe	14 000 Oe	σ_0 (extrapolated)	Coercive field (Oe)	Curie temp. (°K)
$FeBO_3$	1.89	2.45	1.91	11	355
$Fe_{0.978}Al_{0.022}BO_3$	1.84	2.42	1.84	20	346
$Fe_{0.95}Al_{0.05}BO_3$	1.65	2.17	1.67	20	337
$Fe_{0.90}Al_{0.10}BO_3$	1.28	1.86	1.26	34	328
$Fe_{0.79}Al_{0.21}BO_3$	0.18	0.76	0.17	64	~317
$Fe_{0.73}Al_{0.27}BO_3$	0.07	0.61	0.03	75	278
$Fe_{0.97}Ga_{0.03}BO_3$	1.75	2.30	1.71	19	344
$Fe_{0.95}Ga_{0.05}BO_3$	1.58	2.11	1.57		338
$Fe_{0.91}Ga_{0.09}BO_3$	1.00	1.53	0.96	16	324
$Fe_{0.80}Ga_{0.20}BO_3$	0.06	0.55	0.03	12	—
$Fe_{0.69}Ga_{0.31}BO_3$	0.034	0.482	—	—	—
$Fe_{0.60}Ga_{0.40}BO_3$	0.032	0.455	—	—	—
$Fe_{0.51}Ga_{0.49}BO_3$	0.029	0.418	—	—	—
$Fe_{0.41}Ga_{0.59}BO_3$	0.026	0.374	—	—	—
$Fe_{0.21}Ga_{0.79}BO_3$	0.016	0.222	—	—	—
$Fe_{0.993}In_{0.007}BO_3$	1.75	2.34	1.79	23	353
$Fe_{0.978}In_{0.022}BO_3$	1.49	2.11	1.57	168	347
$Fe_{0.92}In_{0.08}BO_3$	0.93	1.55	1.01	150	328
$Fe_{0.87}In_{0.13}BO_3$	0.21	0.77	0.18	235	308
$Fe_{0.74}In_{0.26}BO_3$	0.042	0.519	—	—	245
$Fe_{0.62}In_{0.38}BO_3$	0.040	0.469	—	—	175
$Fe_{0.51}In_{0.49}BO_3$	0.03	0.41	—	—	—
$Fe_{0.43}In_{0.57}BO_3$	0.025	0.373	—	—	—
$Fe_{0.42}In_{0.58}BO_3$	0.02	0.35	—	—	—
$Fe_{0.35}In_{0.65}BO_3$	0.02	0.30	—	—	—
$Fe_{0.15}In_{0.85}BO_3$	0.012	0.155	—	—	—
$Fe_{0.042}In_{0.958}BO_3$	—	0.03	—	—	—
$Fe_{0.98}Cr_{0.02}BO_3$	1.77	2.30	1.76	13	350
$Fe_{0.95}Cr_{0.05}BO_3$	1.61	2.14	1.60	18	343
$Fe_{0.89}Cr_{0.11}BO_3$	1.27	1.80	1.26	23	325
$Fe_{0.80}Cr_{0.20}BO_3$	0.44	0.98	0.40	29	310
$Fe_{0.70}Cr_{0.30}BO_3$	0.046	0.563	—	—	291
$Fe_{0.60}Cr_{0.40}BO_3$	0.04	0.56	—	—	250
$Fe_{0.50}Cr_{0.50}BO_3$	0.041	0.565	—	—	240
$Fe_{0.50}Cr_{0.50}BO_3$	0.04	0.56	—	—	—
$Fe_{0.40}Cr_{0.60}BO_3$	0.04	0.59	—	—	—
$Fe_{0.19}Cr_{0.81}BO_3$	0.045	0.627	—	—	—
$Fe_{0.05}Cr_{0.95}BO_3$	0.05	0.69	—	—	—
$Fe_{0.995}Mn_{0.005}BO_3$	1.94	2.48	1.94	11	352
$Fe_{0.989}Mn_{0.011}BO_3$	1.83	2.35	1.82	22	351
$Fe_{0.979}Mn_{0.021}BO_3$	1.80	2.32	1.80	15	353
$Fe_{0.95}Mn_{0.05}BO_3$	1.66	2.20	1.64	32	348
$Fe_{0.92}Mn_{0.08}BO_3$	1.57	2.13	1.58	26	349

$Fe_{1-x}Ga_xBO_3$, and $Fe_{1-x}Mn_xBO_3$ series. In all of these $Fe_{1-x}M_xBO_3$ solid solutions, the saturation magnetization is seen to decrease with increased M concentration, eventually resulting in paramagnetic materials at the 20 or 30% substitution level. In those samples showing ferrimagnetic behavior, saturation occurs above 500 Oe. The linear behavior in the high-field region is a consequence of the induced increase in the cant angle with increasing applied field. Values of the intrinsic saturation magnetization σ_0 are obtained by extrapolating the linear region to zero applied field and are listed in Table II for all $Fe_{1-x}M_xBO_3$ samples together with the observed magnetizations at 1000 and 14 000 Oe.

In Fig. 7 we show the low-field magnetization curves of the room-temperature ferrimagnetic members of the $Fe_{1-x}In_xBO_3$ series. In contrast to the other solid solution materials, this series shows a large change in crystallite size and habit with increasing In content. Pure $FeBO_3$ powders have a planar habit with crystallites up to 100 μm across while the $Fe_{0.87}In_{0.13}BO_3$ powders are much finer (below 2 μm in size) and have a nearly equidimensional habit.

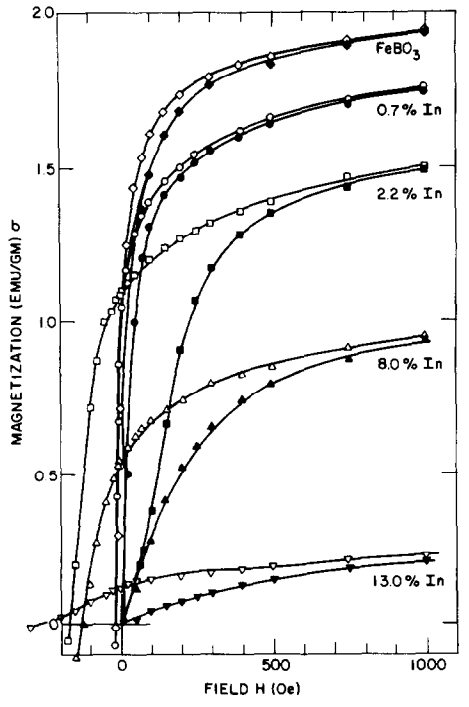

FIG. 7. Low-field magnetization curves at room temperature for ferrimagnetic members of $Fe_{1-x}In_xBO_3$ series.

One can see from Fig. 7 that the magnetization decreases with increasing In concentration. This is due to the combined effects of dilution and the lowering of the Curie temperature brought about by increased In^{3+} ion substitution. The diamagnetic In^{3+} ions do not participate in the magnetic ordering of spins, thereby diluting the spins and causing a local disruption of the magnetic sublattice. We also see from Fig. 7 that the approach to saturation becomes slower and the coercive force becomes larger as the In^{3+} ion concentration is increased. The last two effects are due primarily to the decreasing particle size and increasingly equidimensional habit as has been shown in other magnetic small particle systems. The decreasing T_c value also contributes to these effects but as a secondary effect relative to size and shape effects. The coercivities of all the room-temperature ferrimagnetic $Fe_{1-x}M_xBO_3$ solid solutions are also listed in Table II.

In Fig. 8, the σ_M values[2] at room temperature are plotted for the various $Fe_{1-x}M_xBO_3$ phases as a function of the M concentration. Again, the effects of dilution and T_c lowering are apparent in all five systems, and beyond the 20–30% substitution range all of the materials show paramagnetic behavior at room temperature.

The curve for the In solid solution in Fig. 8 shows the most rapid decrease in magnetization, and one could argue that this can be explained on the basis of the larger ionic radius of In^{3+} compared to the other substituting metal ions. The larger unit-cell parameters of the $Fe_{1-x}In_xBO_3$ phases would be expected to give rise to an increase in the Fe–O distance which would cause a weakening in the superexchange interactions. However, the situation is complicated due to the differences in the pre-

[2] σ_M values are the molar saturation magnetizations defined by the relation: $\sigma_M = (MW)\sigma_0$ where MW is the molecular weight.

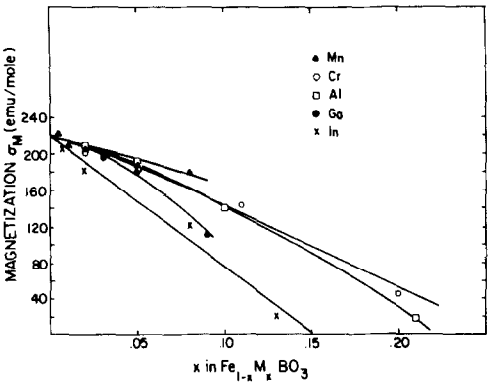

FIG. 8. Molar saturation magnetization σ_M as a function of x in the various $Fe_{1-x}M_xBO_3$ solid solutions at room temperature.

ferred orientation of the various samples already mentioned above. A more detailed analysis of Fig. 8 would require that all of the magnetization values were measured on truly randomly oriented powders or larger single crystals.

In Fig. 9, we give the room-temperature susceptibilities of the paramagnetic $Fe_{1-x}M_xBO_3$ solid solutions for M = Cr, Ga, and In. The nontransition metal ion substituents (In, Ga) show the expected dilution effect and above $x = 0.80$ exhibit the paramagnetic Curie behavior of isolated Fe^{3+} ions in a nonmagnetic matrix. This is seen from Fig. 9, where the dashed line represents the calculated susceptibilities of $Fe_{1-x}In_xBO_3$, assuming Curie behavior with $\mu_{eff} = 5.9$ for Fe^{3+}. In the

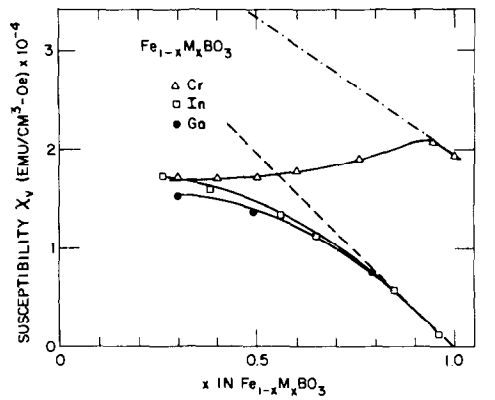

FIG. 9. Room-temperature volume susceptibility of paramagnetic $Fe_{1-x}M_xBO_3$ solid solutions as a function of x.

range $x = 0.30$ to $x = 0.80$, the In and Ga solid solutions have susceptibilities which obey the Curie–Weiss law, with large negative Curie–Weiss constants θ indicating short-range antiferromagnetic exchange interactions between the Fe^{3+} ions.

The situation is more complex for the $Fe_{1-x}Cr_xBO_3$ system. The Cr^{3+} ion has an effective moment of 3.8 μ_B (Fe^{3+}–5.9 μ_B). Assuming no exchange interactions between the transition metal ions, it is expected that the susceptibility would show a continuous decrease with increased Cr^{3+} content down to the $CrBO_3$ end member. It is found, however, that the susceptibility in fact increases slightly with Cr^{3+} concentration, reaching a maximum around $Fe_{0.05}Cr_{0.95}BO_3$. These anomalous results may indicate the presence of strong antiferromagnetic exchange interactions between the transition metal ions in the range $x = 0.30$ to $x = 0.80$. Note that only in the range $x = 0.95$ to $x = 1.0$ do we find Curie behavior to a good approximation. This is seen from the dot-dash line in Fig. 9, which represents the calculated susceptibilities for $Fe_{1-x}Cr_xBO_3$ on the assumption of ideal Curie behavior.

The Curie temperatures were determined for a large number of $Fe_{1-x}M_xBO_3$ samples and are listed in Table II. In this study, we have taken the Curie temperature as the intersection of the paramagnetic component with the steepest slope of the ferrimagnetic part of the magnetization curve. For $FeBO_3$ our value (355°K) is approximately 7°K above the reported single-crystal value (*3*). Better agreement with the single-crystal data is obtained if T_c is taken at the inflection point.

In Figs. 10 and 11, we show the Curie temperatures of the $Fe_{1-x}M_xBO_3$ phases as a function of the concentration of M. The materials containing the nonmagnetic ions (Al^{3+}, Ga^{3+}, In^{3+}) show a more rapid decrease in T_c with increasing x than those containing the transition metal ions (Mn^{3+}, Cr^{3+}). The Curie temperature T_c is directly proportional to the exchange interaction between neighboring spins: $T_c \propto 2S(S+1)\sum_i z_i J_i/3k$, where

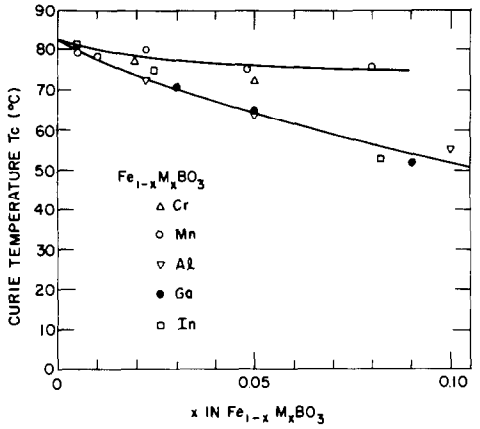

FIG. 10. Curie temperature of $Fe_{1-x}M_xBO_3$ (M = Cr, Mn, Al, Ga, In) as a function of x.

z is the number of ith nearest neighbors (*37*). In $FeBO_3$ the antiferromagnetic alignment of the Fe^{3+} spins is through a superexchange interaction mediated by oxygen ions. The superexchange interactions are dependent on the Fe–O–Fe distance and angle. The nonmagnetic ions (Al^{3+}, Ga^{3+}, In^{3+}) decrease the superexchange interaction by a dilution effect. The decrease is less with the magnetic ions Mn and Cr, indicating participation of these ions in the superexchange coupling.

The low-temperature magnetization behavior in an applied field of 10 kOe of the $Fe_{1-x}In_xBO_3$ samples is shown in Fig. 12. As seen in Fig. 12, with increasing In substitution, the magnetization and Curie temperatures both show a decrease but the materials remain canted antiferromagnets at least up to the $Fe_{0.62}In_{0.38}BO_3$ composition. The large rise in σ at low temperatures, which is already apparent for $Fe_{0.62}In_{0.38}BO_3$, becomes very steep for the $Fe_{0.43}In_{0.57}BO_3$ composition. This phenomenon is thought to be associated with the increasing number of isolated Fe^{3+} ions which show a paramagnetic $1/T$ behavior. The $Fe_{0.43}In_{0.57}BO_3$ sample shows no obvious Curie temperature, but does display ferrimagnetic behavior at very low temperatures. At this composition, the material probably contains small regions of canted antiferromagnetically coupled Fe^{3+} ions immersed in a matrix of In^{3+} and isolated Fe^{3+} ions. More detailed low-temperature magnetic studies are in progress.

In Fig. 13 we present the magnetization curves as a function of temperature for several $Fe_{1-x}Cr_xBO_3$ samples. Again the magnetization at 10 kOe and Curie temperatures decrease with increased Cr^{3+} concentration; however, here the decrease is more gradual than for the $Fe_{1-x}In_xBO_3$ compounds, and canted antiferromagnetic behavior is found for all samples. The magnetization curves for $Fe_{1-x}Cr_xBO_3$ samples in the range $0.4 \leq x \leq 0.6$ show an anomalous temperature dependence with a shallow maximum. In the $Fe_{0.5}Cr_{0.5}BO_3$ sample this maximum is at

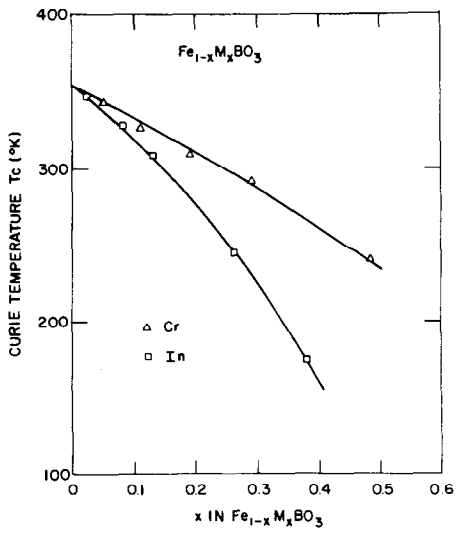

FIG. 11. Curie temperature of $Fe_{1-x}M_xBO_3$ (M = Cr, In) as a function of x.

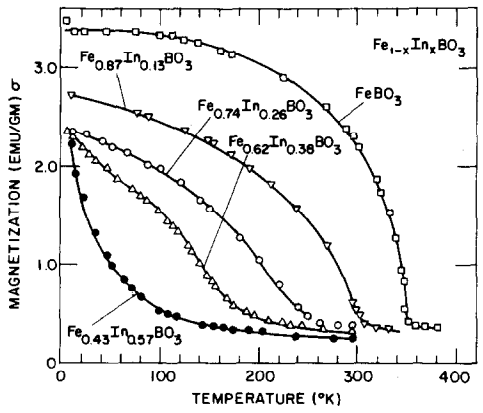

FIG. 12. Magnetization as a function of temperature for the $Fe_{1-x}In_xBO_3$ solid solution series at 10 kOe.

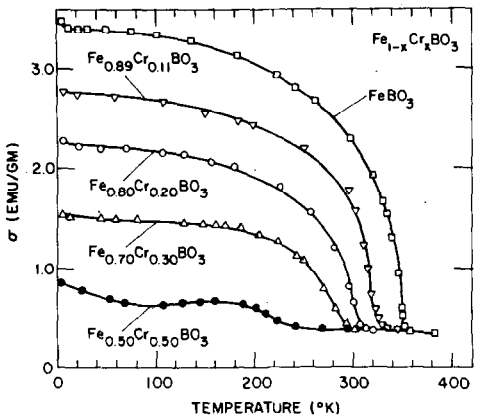

FIG. 13. Magnetization as a function of temperature for the $Fe_{1-x}Cr_xBO_3$ solid solution series at 10 kOe.

175°K. This behavior is similar to that displayed by some $(Fe_{1-x}Cr_x)_2O_3$ compositions, where the existence of several different magnetic structures has been demonstrated (*38*, *39*). More detailed magnetic studies on these $Fe_{1-x}Cr_xBO_3$ phases are in progress and will be the subject of a future paper.

Summary

A systematic study has been made of solid solutions of the type $Fe_{1-x}M_xBO_3$ where M = Mn, Cr, Al, Ga, or In. Complete solid solution ranges ($x = 0$ to 1.0) have been found for M = Cr, Ga, In, whereas the solid solubility is more limited for M = Al ($x = 0$ to 0.32) and Mn ($x = 0$ to 0.10). All materials were prepared in polycrystalline form by the slow evaporation of the appropriate nitrate solutions to which a 400% excess of boric acid has been added. The resulting dry crust was then preheated for 12 hr at 500°C and fired under various conditions in air, typically at 810°C for 3 weeks.

The average crystal size and habit varied from sample to sample with the largest crystallites (10–150 μm across, with a platy habit) found near the $FeBO_3$ composition and the smallest materials (equidimensional habit, 2 μm or less) found for $Fe_{1-x}In_xBO_3$ ($0.13 \leq x \leq 0.95$).

DTA results indicate that for M = Cr, Al, and In the phases become thermally more stable with increasing concentration of M. For M = Ga, the decomposition temperatures go through a broad maximum around $x = 0.40$. Unit-cell parameters have been obtained and plotted for many $Fe_{1-x}M_xBO_3$ samples, giving close agreement with Vegard's law.

The room-temperature saturation magnetization of all the $Fe_{1-x}M_xBO_3$ solid solutions showed diminution with increased substituent concentration. Up to concentrations of 20 to 30% M, the materials showed canted antiferromagnetic behavior at room temperature. Above this substituent concentration range the compounds exhibited paramagnetism. The Curie temperatures also decreased monotonically as a function of substituent concentration, with the nonmagnetic ion (In, Al, Ga) substituted materials exhibiting a more rapid decrease than those with transition metal ions (Mn, Cr). The decrease in saturation magnetization of the $Fe_{1-x}M_xBO_3$ materials is assumed to be due primarily to a dilution effect which eventually disrupts the long-range antiferromagnetic order of the lattice. If the various substituents affected the magnitude of the cant angle, it was a very small change and not obvious from the room-temperature magnetization measurements.[3]

The $Fe_{1-x}M_xBO_3$ solid solutions with M = In, Ga display Curie–Weiss behavior at room temperature with large negative values of θ in the 30 to 80% concentration range. For $Fe_{1-x}In_xBO_3$, below the Curie temperature, there is a significant rise in the magnetization with decreasing temperature, which becomes more pronounced with increased In substitution. One can speculate that this behavior is related to the development of an inhomogeneous magnetic lattice in which regions of canted antiferromagnetically ordered Fe^{3+} ions coexist with regions containing In^{3+} and relatively isolated nonordered Fe^{3+} ions. The rise in magnetization at low temperatures is associated with the paramagnetic behavior of the nonordered Fe^{3+} ions.

[3] However, our recent low-temperature magnetic studies of the $Fe_{1-x}Al_xBO_3$ series show evidence of an increase in cant angle with increasing x at very low temperatures. Details will be presented in a later paper.

The magnetic behavior of the $Fe_{1-x}Cr_xBO_3$ materials in the range $0.3 < x < 0.8$ is rather unusual and indicates possible exchange interactions between the Cr^{3+} and the Fe^{3+} ions. The room-temperature paramagnetic susceptibility in this range is much lower than expected and is found to increase with Cr concentration, reaching a maximum at $x = 0.95$. The low-temperature magnetic behavior of the $Fe_{0.50}Cr_{0.50}BO_3$ compound exhibits an anomalous maximum in its magnetization at approximately 175°K. The Cr^{3+} ions are apparently involved in the magnetic long-range order and the anomalous behavior is presumably due to Cr^{3+}-induced changes in the magnetic order of the lattice. More detailed magnetic studies of the $Fe_{1-x}Cr_xBO_3$ series in the high Cr^{3+} ranges are now in progress and will be reported in a later paper.

Acknowledgments

Most of the analytical services were provided by J. Check, O. McFarland, and W. Rand.

References

1. I. Bernal, C. W. Struck, and J. G. White, *Acta Crystallogr.* **16**, 849 (1963).
2. J. C. Joubert, T. Shirk, W. B. White, and R. Roy, *Mater. Res. Bull.* **3**, 671 (1968).
3. A. J. Kurtzig, R. Wolfe, R. C. LeCraw, and J. W. Nielsen, *Appl. Phys. Lett.* **14**, 350 (1969).
4. R. C. LeCraw, R. Wolfe, and J. W. Nielsen, *Appl. Phys. Lett.* **14**, 352 (1969).
5. R. Wolfe, A. J. Kurtzig, and R. C. LeCraw, *J. Appl. Phys.* **41**, 1218 (1970).
6. I. S. Edelman and A. V. Malakhovskii, *Opt. Spektrosk.* **35**, 959 (1973); English transl: *Opt. Spectrosc.* **35**, 554 (1973).
7. I. S. Edelman, A. V. Malakhovskii, T. I. Vasileva, and V. N. Seleznev, *Fiz. Tverd. Tela* **14**, 2810 (1972); English transl: *Sov. Phys. Solid State* **14**, 2442 (1973).
8. A. V. Malakhovskii and I. S. Edelman, *Phys. Status Solidi (b)* **74**, K145 (1976).
9. N. M. Salanskii, Y. M. Fedorov, A. A. Leksikov, and V. V. Rudenko, *Opt. Spectrosc.* **41**, 58 (1976).
10. N. Koshizuka, T. Okuda, M. Udagawa, and T. Tsushima, *J. Phys. Soc. Japan* **37**, 354 (1974).
11. K. Ozawa and S. Koide, *J. Phys. Soc. Japan* **35**, 754 (1973).
12. I. W. Shepherd, *J. Appl. Phys.* **42**, 1482 (1971).
13. I. W. Shepherd, *Phys. Rev. B* **5**, 4524 (1972).
14. A. E. Meixner, R. E. Dietz, and D. L. Rousseau, *Phys. Rev. B* **7**, 3134 (1973).
15. W. Jantz, J. R. Sandercock, and W. Wettling, *J. Phys. C* **9**, 2229 (1976).
16. J. Haisma, H. J. Prins, and K. L. L. van Mierloo, *J. Phys. D* **7**, 162 (1974).
17. R. Diehl, A. Räuber, and F. Friedrich, *J. Cryst. Growth* **29**, 225 (1975).
18. H. Makram, L. Touron, and J. Loriers, *J. Cryst. Growth* **13/14**, 585 (1972).
19. R. I. Zvereva, E. L. Dukhovskaya, and Y. L. Sapozhnikov, *Izv. Akad. Nauk SSSR. Neorg. Mater.* **11**, 282 (1975). English transl: *Inorg. Mater.* **11**, 236 (1975).
20. R. Diehl, *Solid State Commun.* **17**, 743 (1975).
21. M. Pernet, D. Elmaleh, and J. C. Joubert, *Solid State Commun.* **8**, 1583 (1970).
22. M. P. Petrov, G. A. Smolensky, A. P. Paugurt, and S. A. Kizhaev, *AIP Conf. Proc.* **5**, 379 (1971), Amer. Inst. of Physics.
23. N. M. Salanskii, E. A. Glozman, and V. N. Seleznev, *Zh. Eksp. Teor. Fiz.* **68**, 1413 (1975), English transl: *Soviet Phys. JETP* **41**, 704 (1975).
24. N. M. Salanskii, E. A. Glozman, and V. N. Seleznev, *Phys. Status Solidi (a)* **36**, 779 (1976).
25. M. Eibschütz, L. Pfeiffer, and J. W. Nielsen, *J. Appl. Phys.* **41**, 1276 (1970).
26. T. A. Bither and H. S. Young, *J. Solid State Chem.* **6**, 502 (1973).
27. J. G. White, A. Miller, and R. E. Nielsen, *Acta Crystallogr.* **19**, 1060 (1965).
28. J. Jach, *J. Nonmetals* **2**, 89 (1974).
29. S. C. Abrahams, J. L. Bernstein, P. Gibart, M. Robbins, and R. C. Sherwood, *J. Chem. Phys.* **60**, 1899 (1974).
30. H. Scholze, *Z. Anorg. Allg. Chem.* **284**, 272 (1956).
31. J. J. Capponi, J. Chenavas, and J-C. Joubert, *Bull. Soc. Fr. Mineral. Crist.* **95**, 412 (1972).
32. N. C. Tombs, W. J. Croft, and H. C. Mattraw, *Inorg. Chem.* **2**, 872 (1963).
33. T. A. Bither, C. G. Frederick, T. E. Gier, J. F. Weiher, and H. S. Young, *Solid State Commun.* **8**, 109 (1970).
34. E. M. Levin, R. S. Roth, and J. B. Martin, *Amer. Mineral.* **46**, 1030 (1961).
35. R. D. Shannon and C. T. Prewitt, *Acta Crystallogr. Sect. B* **25**, 925 (1969); *B* **26**, 1046 (1970); *A* **32**, 751 (1976).
36. M. Moriya, "Magnetism I", pp. 81–125, Academic Press, New York (1963).
37. J. S. Smart, "Magnetism III", pp. 63, Academic Press, New York (1963).
38. D. E. Cox, W. J. Takei, and G. Shirane, *J. Phys. Chem. Solids* **24**, 405 (1963).
39. T. Birchall and A. F. Reid, *J. Solid State Chem.* **13**, 351 (1975).